Optimization of magnetic flux density in electrical steels: Slater-Pauling pattern repetition in multicomponent alloys

Seung Su Baik,[1,*] S. K. Kwon,[2] and B. I. Min[1,†]

[1]*Department of Physics, PCTP, Pohang University of Science and Technology, Pohang 790-784, Korea*

[2]*Graduate Institute of Ferrous Technology, Pohang University of Science and Technology, Pohang 790-784, Korea*

(Received 7 September 2011; revised manuscript received 24 November 2011; published 24 February 2012)

By investigating the magnetization variation of Fe-rich multicomponent alloys with solute concentration, the magnetic flux density of Si electrical steel is optimized with average valency. For binary alloys of Fe-X [X = d–5d transition-metal (TM) and 3sp–6sp elements], the usual mountain-shape behavior of the Slater-Pauling curve is produced even for late 4d–5d TM, and the monotonically decreasing behavior for 3sp–5sp elements. Anomalously, a rise-and-fall pattern is found for the 6sp element of X = Bi. For ternary alloys of Fe-Si-X (X = 3d–5d TM and 3sp–6sp elements), the role of Si is shown to shift the starting point of moment variation and the magnetic flux density of Fe-Si-X alloys is found to repeat the Si-absent binary pattern at the shifted reference moment. On the basis of the calculated magnetic moments, Fe-Si-X-Y (X = Co, Pd, Pt and Y = Al, Sb, Bi) is proposed as a viable candidate for the optimum products of electrical steels.

DOI: 10.1103/PhysRevB.85.052402 PACS number(s): 75.50.Bb, 75.30.Cr, 81.05.Zx

I. INTRODUCTION

Si electrical steels are widely used soft magnetic materials in energy transferring devices, such as motors, generators, and transformers. Today, the growing energy demand in industry and everyday life requires a higher standard of energy efficiencies in power generating and consuming equipment. To achieve such a requirement, the design of electrical steels has been directed to pursue two magnetic properties. The first is high permeability to maximize the response to the applied field and the second is low core loss to minimize the energy dissipation. A small addition of Si up to ∼3.3 wt. % (weight percent) to bcc iron (α-Fe) is known to be a solution to meet both requirements.[1–9] Since Si acts as a grain-size enhancer, the high permeability can be achieved via lowered magnetic anisotropy. The increased electrical resistivity by Si addition causes an eddy current decrement and lessens the total energy loss. On the debit side, however, Si alloying reduces the saturation magnetic flux density due to the nonmagnetic nature of Si. Therefore, while keeping Si as a primary solute, searching for the proper additional alloying elements that can recover the lost flux density is urgently demanded in the design of electrical steels.

Designing new magnetic materials requires the adjustment of many physical and engineering parameters that are sensitively correlated with one another.[4,5,10] Extensive efforts have been made to investigate the ferromagnetism of intermetallic alloys with transition-metal (TM) hosts. As a result, the behavior of magnetic moments of 3d TM binary alloys was explained by the celebrated Slater-Pauling curve,[1,11,12] which exhibits the mountain-shape magnetization variation with average valency. The elegantly simple feature of the Slater-Pauling curve bears many broad and profound implications. The saturation moment reflects the number of bonding electrons in localized d manifolds, which imparts the binding strength of constituent atoms alongside mobile s electrons. Hence, the single parameter formulation of a series of alloys with saturation moments can afford to predict other physical properties, such as compressibility, hardness, ductility, melting point, and magnetic transition temperature.[11,12] Ironically, the underlying mechanism of metallic ferromagnetism is yet controversial even for pure α-Fe and the theoretical models of intermetallics are still more complicated.[13–25] As a starting point, however, Slater's spirit of simplification, "the only effect of going from pure metal to alloy is to change the average number of valence electrons," is still illuminating as long as the alloy's magnetic properties are concerned.

In this Brief Report, we explore the general features of magnetic saturations of Fe-rich alloys, Fe-X and Fe-Si-X, with a single parameter of average valency. The solute species is extended from 3d TM through late 4d–5d TM to late 3sp–6sp elements. After the inspection of various binary and ternary alloys, we visualize the regularity of magnetizations and define the alloying effects in Si electrical steels in terms of binary pattern reproduction. Further, we describe the alloying effects beyond ternary alloys. The results lead to promising applications in improving the magnetic flux density of electrical steels.

II. COMPUTATIONAL METHODS

We have employed the first-principles full-potential linearized augmented plane-wave (FLAPW) method[26] implemented in the WIEN2K code.[27] The generalized gradient approximation (GGA)[28] was used for the exchange-correlation potential. The muffin-tin (MT) radius of each atomic species was chosen between 2.0∼2.3 a.u. depending on the atomic radius. The wave functions inside MT spheres were expanded in spherical harmonics up to $l = 10$, and in the interstitial regions with plane waves up to $K_{\max} = 4.0$.[29,30] Charge densities were described with plane waves up to $G_{\max} = 16\sqrt{\text{Ry}}$. In all calculations, volume optimizations with atomic relaxations were performed until the forces at every atomic site became less than 1.0 mRy/a.u.. We have used 50 000 **k** points inside the Brillouin zone for the single conventional bcc cell of pure Fe. As the supercell size increases by $N_1 \times N_2 \times N_3$ times, the corresponding **k** points have been applied in the way of $1/N_1 \times 1/N_2 \times 1/N_3$ reduction. For self-consistency, the energy and the charge convergence criteria were adopted as 1.0×10^{-5} Ry and 1.0×10^{-4} e/a.u.^{3}, respectively.

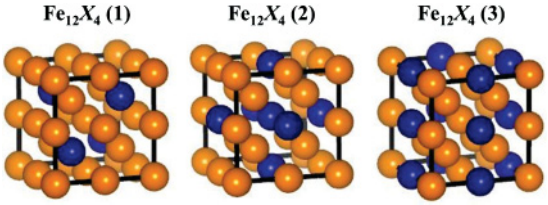

FIG. 1. (Color online) Three different atomic configurations for the $2 \times 2 \times 2$ supercell with 12.5 at. % of solutes. Orange and blue spheres represent the host (Fe) and the solute (X) atoms, respectively.

To simulate the disorder effects, the magnetic moments were averaged for the selected $2 \sim 3$ atomic configurations at each solute composition level. Supercells were chosen according to the smallest cell scheme, in which solute atoms were positioned for supercells to have as high a symmetry as possible. For example, the smallest cell which can be made for the solute concentration of 1.85 at. % is the $3 \times 3 \times 3$ supercell. The smallest for 6.25 at. % is $2 \times 2 \times 2$, and for 9.38 at. % is $2\sqrt{2} \times 2\sqrt{2} \times 2$, and so forth. The solute atoms are substituted into the high-symmetry sites first. When we construct a different atomic configuration, the crystal symmetry is lowered in some cases. For example, when we construct a supercell with 12.5 at. % of solutes, the simplest and smallest supercell available is the $2 \times 2 \times 2$ supercell in which the first solute atom is located at the cell center and the second is at the corner. If we locate the second solute at the face center instead of at the corner, the crystal symmetry becomes tetragonal. The cell size is doubled only in the case that a different atomic configuration cannot be made with the given supercell. Figure 1 shows an example for the $2 \times 2 \times 2$ supercell with 12.5 at. % of solutes, for which three different atomic configurations are considered in the calculation. The largest supercell we have considered for the solute concentration of 0.78 at. % corresponds to $4 \times 4 \times 4$ supercell, which includes 128 sites.

III. Fe-X ($X = 3d$–$5d$ TM ELEMENTS)

Figure 2 shows the variation of average magnetic moment per atom (M_{av}) with average valency (Z_v) for binary alloys of Fe-X ($X = 3d$–$5d$ TM). The solute concentrations vary from 0 to 31 at. %, which is rearranged from 8.0 to 8.5 in Z_v conversion. Clearly, the magnetic saturation of late $4d$–$5d$ TM alloys exhibits the usual mountain-shape behavior of the Slater-Pauling curve, which is originally derived from $3d$ TMs only. As a common feature, M_{av} increases almost linearly up to $Z_v \sim 8.13$ with slightly different line slopes. Reminding the reader that pure Rh, Pd, Ir, and Pt are paramagnetic elements with broad $4d$ and $5d$ bands, we note that this increasing magnetization with increasing solute is intriguing because a diametric phase mixture results in the gradual enhancement of effective exchange field splitting in the total density of states. As the solute concentration increases, M_{av} reaches a maximum at $Z_v \sim 8.2$ except for Rh and Ir, and slowly falls off. The peak values in Fig. 2 read $M_{\text{av}} \sim 2.33$, 2.29, 2.33, 2.37, 2.27, and 2.37 μ_{B} for $X =$ Co, Ni, Rh, Pd, Ir, and Pt, respectively. Based on the shown data, one may order the effectiveness for the saturation moment enhancement in Fe-X as Pt $\geqslant$ Pd $>$ Co $\approx$ Rh $>$ Ni $>$ Ir. This ordering implies that paramagnetic elements Pd and Pt are more effective than ferromagnetic elements Co and Ni. Overall, the highest value of $M_{\text{av}} \sim 2.37$ μ_{B} is achieved with $X =$ Pd and Pt[1,31] at $Z_v \sim 8.19$, which is about 10% larger than 2.16 μ_{B} of pure α-Fe.

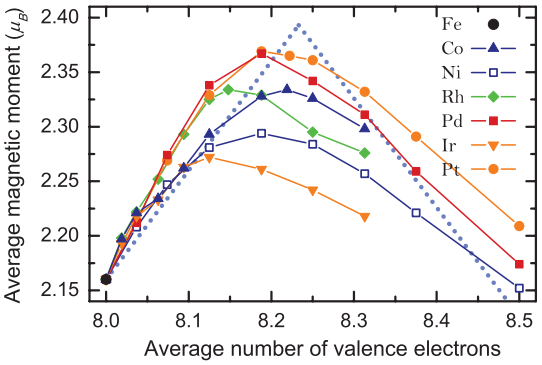

FIG. 2. (Color online) Average magnetic moment per atom (M_{av}) in units of μ_{B} versus average valency (Z_v) for binary alloys of Fe-X ($X = 3d$–$5d$ TM). Dashed blue lines represent the predicted two branches with $\pm 45^\circ$ slopes from the ideal Slater-Pauling curve.

Figure 3 provides the magnetic moment inside the Fe MT-sphere as a function of X-Fe distance for binary alloys of Fe-X ($X =$ Co, Ni, Rh, Pd, Ir, and Pt). For comparison, three solute concentrations are chosen as $x = 0.78$, 1.85, and 6.25 at. %. The shown data have been adopted from a single atomic configuration at each solute content, in which the solute atom has been positioned at the cell center. This spatial distribution of moment perturbation provides a physical rationale to elucidate how the ascending moment saturation is produced even for late $4d$–$5d$ TM alloys. As a common feature at low solute content of $x = 0.78$ at. %, the enhanced spin-polarization of host Fe is a rapidly decreasing function of X-Fe distance up to the third nearest neighbor[23] and shows oscillating behavior, which is reminiscent of RKKY-type oscillation.[32] The perturbed spin imbalance of the first nearest Fe affects the second nearest Fe, which again perturbs the spin density of the third nearest Fe and so forth. Hence, it seems that the chain-reaction-like long-range interactions occur. The increased solutes of $x = 1.85$[33] and 6.25 at. % show larger oscillation amplitudes caused by stronger solute-solute interactions. As the solute content increases, the nearby Fe atoms to one solute are more easily affected by another solute. As clearly seen, the elements with 10 valence [Figs. 3(b), 3(d), and 3(f)] induce the stronger spin density of localized Fe d shells than the elements with 9 valence [Figs. 3(a), 3(c), and 3(e)]. However, the maximum saturation moment of Fe-Co in Fig. 2 is larger than that of Fe-Ni. The reason is understood from the magnetic moment of the solute itself. At maximum peaks in Fig. 2, the moment difference between Co and Ni solute reaches 0.83 μ_{B}. Although the induced spin-density of the Fe host in Fe-Ni is stronger than that in Fe-Co, this solute moment difference is too large to be exceeded by the enhanced Fe moments in Fe-Ni.

Compared with the magnetic moments of 1.60 μ_{B} for pure Co and 0.63 μ_{B} for pure Ni, the solute moments of 1.79 μ_{B} for Co and 1.00 μ_{B} for Ni at $x = 0.78$ at. % are, respectively, 11.5% and 59.4% increased values. Notably,

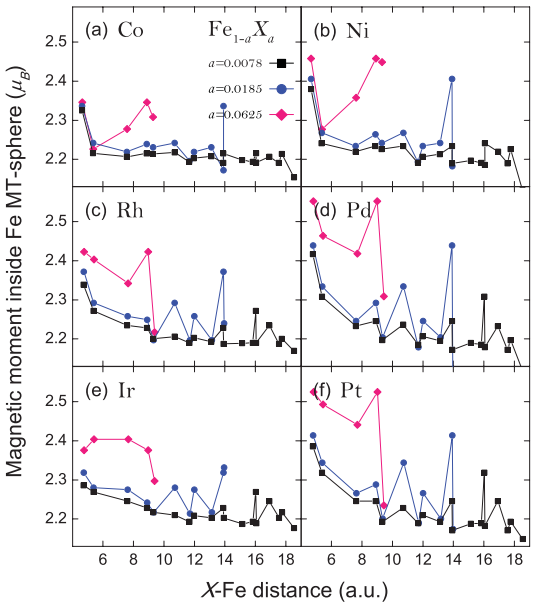

FIG. 3. (Color online) Magnetic moment inside Fe MT sphere (M_{Fe}) in units of μ_B versus X-Fe distance in units of a.u. for binary alloys of $Fe_{1-a}X_a$ (X = Co, Ni, Rh, Pd, Ir, and Pt, $a = 0.0078$, 0.0185, 0.0625). All Fe atoms inside the radius from solute to the farthest Fe atom are shown.

other nonmagnetic alloying elements also gain relatively small but sizable magnetic saturation. These enhanced or acquired magnetic moments tend to increase with increasing solute contents, and approach the maximum at $Z_v \sim 8.2$. The peak values read ~1.84, 1.01, 0.84, 0.55, 0.61, and 0.56 μ_B for Co, Ni, Rh, Pd, Ir, and Pt, respectively. In this way, the nonmagnetic solutes become magnetic inside the Fe host, and the total magnetization enhancement synergistically occur via host-solute interactions. Considering a similar parametric analysis with average valency, we expect that 4*d* and 5*d* alloying elements of Ru and Os which are isovalent with Fe would result in pure Fe-equivalent magnetic saturation. The magnetization variation of Fe-X (X = Ru and Os) produces a nearly constant moment around 2.16 μ_B up to 9.4 at. % of solutes, and then shows linearly decreasing behavior. Inside the Fe host, the average magnetic moment of Ru varies from 0.36 μ_B to 0.65 μ_B, while Os only from 0.01 μ_B to 0.32 μ_B.

The detailed study given above reveals the general trend of magnetic saturation of Fe-X alloys whose solute species is extended from 3*d* to 5*d* TMs. As a generic feature, the saturation moment shows a rise-and-fall pattern in which both branch lines are within the predicted scope of the ideal Slater-Pauling curve with small slope deviations. For $8.0 < Z_v < 8.2$, Rh, Pd, and Pt are grouped into highly effective alloying elements for moment enhancement, whereas Co and Ni into less effective. This grouping is closely related to the volume expansion rate of Fe-TM alloys with increasing solutes. At maximum peaks in Fig. 2, the volume expansions of Fe-X for X = Rh, Pd, and Pt reach 8.9, 7.7, and 8.2 %, respectively, with respect to the pure Fe volume. In contrast, the volume increments for X = Co and Ni only read 2.0 and 2.4 % at maximum peaks.

IV. Fe-X (X = 3*sp*–6*sp* ELEMENTS)

The successful description of magnetization trends thus far encourages us to examine the possibility of alloying species extension from TM to *sp* elements (SPs). In Fig. 4, we investigate the magnetization variation of Fe-X alloys (X = 3*sp*–6*sp* elements) as a function of Z_v. The solute compositions vary from 0 to 25 at. %, which is transformed from 8.0 to 7.0 in Z_v conversion. As expected from lower valency of SP, the overall behavior of M_{av} is described with a decreasing function of solute contents. Especially, in the dilute region of solutes, $7.9 \lesssim Z_v \leqslant 8.0$, all magnetic saturations are located very close to the extended line of the ideal Slater-Pauling curve. Reminding the reader that pure Si, As, and Sb are classified as metalloid, Al and Bi as metal, and P as nonmetal, we note that this Slater-Pauling-like behavior implies that our single-parameter analysis is quite applicable even to alloys with large potential difference between host and solute, $|\Delta Z| \geqslant 3$. By deviation assessment from the extrapolated Slater-Pauling curve, the observed saturation moments are further classified into two alloy groups. For light 3*sp*–4*sp* elements of X = Al, Si, P, and As, the monotonically decreasing behaviors of magnetic moments retain their decremental form over a wide range of solute concentrations, $7.4 \lesssim Z_v \leqslant 8.0$. Noteworthily, the saturation moment of Fe-Al varies more or less insensitively around $M_{av} \sim 2.1$ μ_B for this solute range. However, for heavy 5*sp*–6*sp* elements of X = Sb[1,15,34] and Bi, the moment variations show somewhat anomalous behaviors. Markedly, Fe-Bi exhibits a rise-and-fall pattern in the solute range of $7.7 < Z_v < 8.0$. The maximum moment of $M_{av} \sim 2.24$ μ_B is reached at $Z_v \sim 7.8$, which is the largest saturation among Fe-SP alloys and even larger than the pure Fe moment.[35] This feature is caused by the volume expansion of Fe-Bi due to the large atomic dimension of Bi. At the corresponding solute content, the volume increment of Fe-Bi amounts to ~10% with respect to the pure Fe volume. Considering that Bi belongs to the last period of the post-TM block, the period 5 to 6 is thought to be the transitional period which may result in a maximum peak on alloying.

In fact, similarly to Bi alloying, other alloying elements also have the volume effects. Three alloys of Fe-X (X = Al, As, and Sb) show continuous volume expansion with

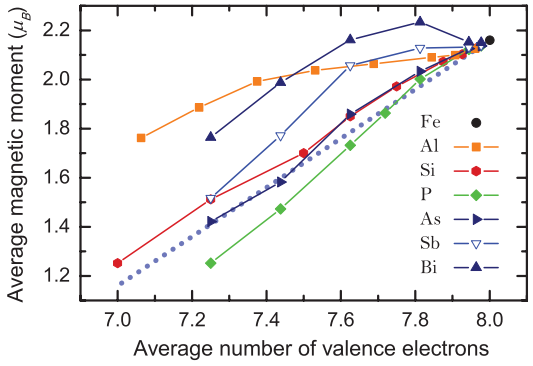

FIG. 4. (Color online) Average magnetic moment per atom (M_{av}) in units of μ_B versus average valency (Z_v) for binary alloys of Fe-X (X = 3*sp*–6*sp* elements). Dashed blue line with +45° slope is extended from the ascending branch of the ideal Slater-Pauling curve.

increasing solute contents, whereas Fe-X (X = Si and P) exhibit volume contraction.[36] However, the volume increasing rates significantly differ from one solute to another. At 12.5 at. % of solutes, the volume increments of Fe-X (X = Al, As, Sb, and Bi) reach 4.0, 3.0, 12.5, and 17.9 %, respectively, with respect to the pure Fe volume.

The saturation behavior in Fig. 4 suggests that special interests can be focused on alloying elements of Al, Sb, and Bi in searching for the optimum products of Si steels. Before going to ternary alloys of Fe-Si-X, we briefly comment on the spatial variation of the Fe-moment perturbation. As in Fe-TM alloys, the magnetic moments of neighboring Fe atoms to solutes show oscillatory behavior. However, a striking difference appears in the first nearest Fe atoms. At low solute contents of $x = 0.78$ and 1.85 at. %, their magnetic moments of $2.01\ \mu_B < M_{Fe} < 2.13\ \mu_B$ are smaller than the pure Fe moment of 2.16 μ_B. Then, the second nearest neighbors restore the lost moments. The overall decremental behavior of saturation moments therefore comes from the small moments of solutes which range from $-0.04\ \mu_B$ to $-0.1\ \mu_B$ inside the host.

V. Fe-Si-X (X = TM, SP ELEMENTS)

Si-alloyed iron is undoubtedly the most popular soft magnetic material with high permeability and high resistivity. The imposed Si content varies in different commercial uses and the choice is specialized on the basis of capital cost and performance. Although a higher Si content would further reduce eddy current loss by increasing resistivity, its maximum content is limited below 3.3 wt. % in normal manufacturing techniques due to the resultant brittleness of Si steel.[9] In Fig. 5, we examine the magnetization variation of ternary alloys of Fe-Si-X (X = TM and SP) with average valency (Z_v). As a primary solute, Si content is fixed at 6.3 at. % which corresponds to ~3.2 wt. %, while the secondary solutes of X = TM and SP vary from 0 to 31 at. %. Due to Si-alloying effect only, the initial moment in the (Z_v, M_{av}) plane is moved from (8.0, 2.16 μ_B) to (7.75, 1.97 μ_B). It is clearly seen that for all secondary solutes, the saturation moment behavior of ternary alloys repeats the Slater-Pauling pattern

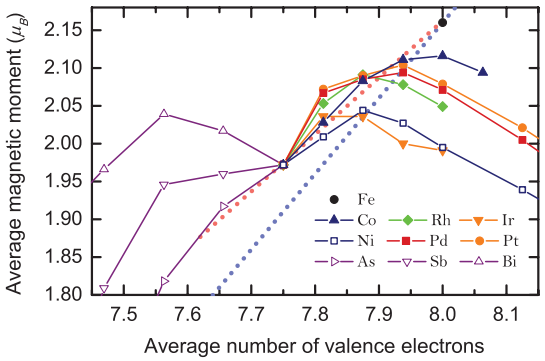

FIG. 5. (Color online) Average magnetic moment per atom (M_{av}) in units of μ_B versus average valency (Z_v) for ternary alloys of Fe-Si-X (X = TM and SP). Dashed blue line with +45° slope is extended from the ascending branch of the ideal Slater-Pauling curve. Dashed red segment is the extension between magnetic moment of pure Fe and magnetic moment of 6.3 at. % Si-alloyed Fe which has no secondary solute.

of the original binary alloy without Si at the shifted reference point of (7.75, 1.97 μ_B). The mountain-shape behaviors for $X = 3d$–$5d$ TMs, a rise-and-fall pattern for X = Bi, and the decremental forms of X = As and Sb are similarly manifested in Fig. 5. However, several detailed differences are found between binary and ternary systems. For Fe-Si-X, Pd or Pt alloying have a slightly weaker impact on the maximum saturation moment in comparison to Co alloying. The peak values read 2.09, 2.11, and 2.12 μ_B for Pd, Pt, and Co, respectively. Also notably, M_{av} of Fe-Si-Bi is comparable to M_{av}'s of Fe-Si-Ni and Fe-Si-Ir, which have the maximum saturation of ~2.04 μ_B. The secondary solute contents that induce the maximum moments are 25.0, 6.3, 18.8, 9.4, 6.3, 9.4, and 6.3 at. % for Co, Ni, Rh, Pd, Ir, Pt, and Bi, respectively.

In a general sense, this pattern reproduction is intriguing because the similar behaviors are found in other multicomponent alloys with different Si content or with different host matrix. When we lower the Si content to 3.1 at. % in the Fe host, the reference moment moves from (Z_v, M_{av}) = (8.0, 2.16 μ_B) to (7.88, 2.06 μ_B). Then, the binary-type behavior is reproduced for the variation of secondary solutes of X = TM and SP. Especially, a rise-and-fall pattern is also found for Fe-Si-Bi with a peak value of 2.17 μ_B, which is comparable to the maximum moment of Fe-Si-Ni. For the hexagonal Co host with 6.3 at. % Si, the control point moves from (9.0, 1.60 μ_B) to (8.69, 1.42 μ_B), and similar behaviors are exhibited. It is accordingly thought that this feature is generic in alloys with a ferromagnetic host and may be roughly understood as a *minimalistic* pattern repetition since they repeat the simplest possible pattern on alloying.

In applications, the magnetic saturations of multicomponent alloys can be quantitatively estimated from the information of binary alloys. When we add a new kind of solute and vary its content with other solute compositions fixed, the induced moment variation is expected to be a nearly binary-type behavior at the shifted reference moment. As a result, by deduction, we compactify the blending effects of a newcomer in existing alloys beyond ternary alloys. Concerning the possible solute candidates to increase the magnetic saturation of Fe-Si-X-Y alloys, late TMs such as Co, Pd, Pt for X and heavy SPs such as Bi for Y are considered to be the best candidates. Considering similar effects in electrical resistivity,[1,6,7] sp elements such as Al and Sb are also recommended for Y since they have the additional benefit of low moment reduction.

VI. CONCLUSION

The parametric analysis with average valency shows that the Slater-Pauling theory is extendable to Fe-rich multicomponent alloys. The broadened alloying options include the solute species of late $3d$–$5d$ TM and late $3sp$–$6sp$ elements. Based on the calculated magnetic moments of Fe-X and Fe-Si-X alloys, we have shown that the magnetization variation of Fe-Si-X alloys can be interpreted as the Si-absent binary alloy pattern repetition at the shifted reference moment. Further, by deduction, we compactified the adding effects of new solute species beyond ternary alloys. We have proposed Fe-Si-X-Y (X = Co, Pd, Pt and Y = Al, Sb, Bi) as a feasible candidate for the magnetically optimized products of electrical steels.

ACKNOWLEDGMENTS

This work was supported by NRF (2009-0079947), the steel science project of POSCO, the Korea-Sweden research cooperation program (KSRCP-2008-08), and the WCU program (R32-2008-000-10147-0) of NRF. Helpful discussions with L. Vitos and O. Y. Kwon are appreciated.

*ssb@postech.ac.kr
†bimin@postech.ac.kr

[1]R. M. Bozorth, *Ferromagnetism* (Van Nostrand, New York, 1953); R. M. Bozorth, *Ferromagnetism* (Wiley-IEEE Press, New York, 1993).
[2]M. F. Littmann, IEEE Trans. Magn. **7**, 48 (1971).
[3]J. W. Shilling and G. L. Houze Jr., IEEE Trans. Magn. **10**, 195 (1974).
[4]G. Y. Chin, Science **208**, 888 (1980).
[5]A. J. Moses, IEE Proc. **137**, 233 (1990).
[6]J. S. Woo and C. S. Lee, J. Korean Inst. Metals **28**, 179 (1990); J. T. Park and J. S. Woo, J. Korean Inst. Met. Mater. **30**, 561 (1992).
[7]R. C. O'handley, *Modern Magnetic Materials: Principles and Applications* (Wiley, New York, 2000).
[8]J. B. Lorenzo, T. Ros-Yanez, M. De Wulf, and Y. Houbaert, IEEE Trans. Magn. **40**, 2739 (2004).
[9]B. D. Cullity and C. D. Graham, *Introduction to Magnetic Materials*, 2nd ed. (Wiley-IEEE Press, Piscataway, NJ, 2009).
[10]G. B. Olson, Science **288**, 993 (2000).
[11]J. C. Slater, J. Appl. Phys. **8**, 385 (1937).
[12]L. Pauling, Phys. Rev. **54**, 899 (1938).
[13]N. F. Mott, Adv. Phys. **13**, 325 (1964).
[14]A. R. Williams, V. L. Moruzzi, A. P. Malozemoff, and K. Terakura, IEEE Trans. Magn. **19**, 1983 (1983).
[15]A. P. Malozemoff, A. R. Williams, and V. L. Moruzzi, Phys. Rev. B **29**, 1620 (1984).
[16]V. I. Anisimov, V. P. Antropov, A. I. Liechtenstein, V. A. Gubanov, and A. V. Postnikov, Phys. Rev. B **37**, 5598 (1988).
[17]B. Drittler, N. Stefanou, S. Blügel, R. Zeller, and P. H. Dederichs, Phys. Rev. B **40**, 8203 (1989).
[18]P. H. Dederichs, R. Zeller, H. Akai, and H. Ebert, J. Magn. Magn. Mater. **100**, 241 (1991).
[19]J. Guevara, V. Vildosola, J. Milano, and A. M. Llois, Phys. Rev. B **69**, 184422 (2004).
[20]M. P. J. Punkkinen, K. Kokko, M. Ropo, I. J. Väyrynen, L. Vitos, B. Johansson, and J. Kollar, Phys. Rev. B **73**, 024426 (2006).
[21]G. Rahman, I. G. Kim, H. K. D. H. Bhadeshia, and A. J. Freeman, Phys. Rev. B **81**, 184423 (2010).
[22]P. Olsson, T. P. C. Klaver, and C. Domain, Phys. Rev. B **81**, 054102 (2010).
[23]M. B. Stearns, Phys. Rev. B **4**, 4081 (1971); **13**, 1183 (1976); **17**, 2809 (1978); M. B. Stearns and J. M. Norbeck, *ibid.* **20**, 3739 (1979).
[24]M. B. Stearns, Phys. Today **31**(4), 34 (1978).
[25]P. Mohn, *Magnetism in the Solid State: An Introduction*, Corrected 2nd Printing (Springer-Verlag, Berlin, 2006).
[26]M. Weinert, E. Wimmer, and A. J. Freeman, Phys. Rev. B **26**, 4571 (1982).
[27]P. Blaha, K. Schwarz, G. K. H. Madsen, D. Kvasnicka, and J. Luitz, WIEN2K, Technische Universität Wien, Austria, 2001.
[28]J. P. Perdew, K. Burke, and M. Ernzerhof, Phys. Rev. Lett. **77**, 3865 (1996).
[29]S. Cottenier, DFT and the Family of (L)APW Methods: A Step-by-Step Introduction, found on the WIEN2K homepage [http://www.wien2k.at/reg_user/textbooks/].
[30]S.-W. Seo, Y. Y. Song, G. Rahman, I. G. Kim, M. Weinert, and A. J. Freeman, J. Magn. **14**, 137 (2009).
[31]M. Fallot, Ann. de physique (Paris) **10**, 291 (1938).
[32]M. A. Ruderman and C. Kittel, Phys. Rev. **96**, 99 (1954); T. Kasuya, Prog. Theor. Phys. (Kyoto) **16**, 45 (1956); K. Yosida, Phys. Rev. **106**, 893 (1960); J. Friedel, Nuovo Cimento Suppl. **7**, 287 (1958); J. H. Van Vleck, Rev. Mod. Phys. **34**, 681 (1962).
[33]M. F. Collins and G. G. Low, Proc. Phys. Soc. London **86**, 535 (1965).
[34]A. T. Aldred, J. Phys. C **1**, 1103 (1968).
[35]The spin-orbit effects on the magnetic moment are found to be similar between the heavy and the light TM and SP elements. The saturation moment increments including the orbital magnetic moment read 0.03 $\sim$ 0.05 μ_B for all binary alloys of Fe-X (X = TM and SP).
[36]H. W. King, J. Mater. Sci. **1**, 79 (1966).